

# SCIENTIFIC REPORTS

OPEN

## An *in-situ* synthesis of Ag/AgCl/TiO<sub>2</sub>/hierarchical porous magnesian material and its photocatalytic performance

Received: 03 November 2015

Accepted: 26 January 2016

Published: 17 February 2016

Lu Yang<sup>1,2</sup>, Fazhou Wang<sup>1</sup>, Chang Shu<sup>2</sup>, Peng Liu<sup>3</sup>, Wenqin Zhang<sup>1</sup> & Shuguang Hu<sup>1</sup>

The absorption ability and photocatalytic activity of photocatalytic materials play important roles in improving the pollutants removal effects. Herein, we reported a new kind of photocatalytic material, which was synthesized by simultaneously designing hierarchical porous magnesian (PM) substrate and TiO<sub>2</sub> catalyst modification. Particularly, PM substrate could be facilely prepared by controlling its crystal phase (Phase 5, Mg<sub>3</sub>Cl(OH)<sub>5</sub>·4H<sub>2</sub>O), while Ag/AgCl particles modification of TiO<sub>2</sub> could be achieved by *in situ* ion exchange between Ag<sup>+</sup> and above crystal Phase. Physiochemical analysis shows that Ag/AgCl/TiO<sub>2</sub>/PM material has higher visible and ultraviolet light absorption response, and excellent gas absorption performance compared to other controls. These suggested that Ag/AgCl/TiO<sub>2</sub>/PM material could produce more efficient photocatalytic effects. Its photocatalytic reaction rate was 5.21 and 30.57 times higher than that of TiO<sub>2</sub>/PM and TiO<sub>2</sub>/imporous magnesian substrate, respectively. Thus, this material and its intergration synthesis method could provide a novel strategy for high-efficiency application and modification of TiO<sub>2</sub> photocatalyst in engineering filed.

TiO<sub>2</sub> photocatalyst has been extensively investigated and commercial application in several fields due to its high redox ability and stability under light illumination<sup>1–4</sup>. However, research on TiO<sub>2</sub> photocatalysis suggested that its constructive and highly effective application remains a series of issues, of which the immobilized performance, visible light response and electron-hole recombination rate were considered to be its developing and application bottlenecks<sup>5,6</sup>. Recently, it was found that Ag/AgX (Br, Cl, I) coupling with TiO<sub>2</sub> photocatalyst revealed a fascinating photocatalytic performance<sup>7–13</sup>. It has been proven that Ag nanoparticles (Ag NPs) can obtain a strong visible light absorption by its Surface Plasmon Resonance (SPR), while AgX/TiO<sub>2</sub> structure is useful for photo-generated charges separation. Based on these principles, Lu *et al.*<sup>14</sup> further enhanced the photocatalytic activity of Ag/AgCl/TiO<sub>2</sub> photocatalyst by using transition metals as a co-catalyst. These reports demonstrated that various photocatalysts with high photocatalytic activity could be easily achieved by its surface modification and doping methods. Therefore, the main concern of these materials applied in practical engineering is seems to seek a reasonable immobilization substrate.

Some 3D interconnected hierarchical porous substrates including metal based, glass based, ceramics based, carbon based and cementitious materials, etc.<sup>15,16</sup>, could provide higher surface area and disperse ability for photocatalyst coating. Most importantly, these substrates may possess an excellent reagents diffusion ability to active sites located inside framework or inter-particulate, thus are beneficial for photocatalysis<sup>17</sup>. However, the production of these substrates usually needs to couple the specific templates or surfactants with high temperature treatment, which make them difficult to regulate. Moreover, the large scale and low cost synthesis methods of these substrates and their combination with the modified photocatalysts also require a further investigation. In that case, the integration design of photocatalysts modification and their coating substrates are very interesting and important for high efficiency photocatalysis and the actual engineering application.

Herein, we presented a new kind of Ag/AgCl/TiO<sub>2</sub>/hierarchical porous magnesian material, which can be conveniently synthesized by simultaneously designing the hierarchical porous magnesian (PM) substrate and

<sup>1</sup>State Key Laboratory of Silicate Materials for Architectures, Wuhan University of Technology, Wuhan 430070, PR China. <sup>2</sup>School of Materials Science and Engineering, Wuhan University of Technology, Wuhan 430070, PR China. <sup>3</sup>School of Chemistry, Chemical Engineering and Life Science, Wuhan University of Technology, Wuhan 430070, PR China. Correspondence and requests for materials should be addressed to F.W. (email: fzhwang@whut.edu.cn)

Ag/AgCl modified TiO<sub>2</sub> photocatalyst. Especially, owing to the physical structure characteristics of phase 5 (Mg<sub>3</sub>Cl(OH)<sub>5</sub>·4H<sub>2</sub>O) crystals, the prepared material offered a well gas diffusion and light transmittance channels for photocatalysis. Meanwhile, by using phase 5 coupling with Ag<sup>+</sup> ion, the light absorption performance and charges transfer properties of prepared materials were further enhanced. Thus, this method and prepared material could provide a new strategy for high-efficiency application of TiO<sub>2</sub> photocatalyst in actual engineering field.

## Results

Owing to the air-solid interface reaction property of photocatalytic process, the substrate surface area, light transmission and gas absorption ability have significant influence on photocatalytic efficiency for supported photocatalytic materials<sup>18,19</sup>. Fig. 1a shows the ESEM images of porous magnesian (PM) substrate. It can be seen that PM substrate are composed of macro air pores, interconnection pores and interlaced network micro-pores, respectively. Interestingly, PM are almost composed by needle-like crystals (phase 5, Mg<sub>3</sub>Cl(OH)<sub>5</sub>·4H<sub>2</sub>O), and therefore forming the 3D network structure and interlaced network micro-pores<sup>20,21</sup>. After incorporating TiO<sub>2</sub> particles, it can be clearly observed that the loose and interpenetration textures were formed between TiO<sub>2</sub> particles and needle like phase 5 crystals (Fig. 1b), which are help for the absorption and photocatalysis of TiO<sub>2</sub> particles. Meanwhile, the facile and low energy consumption synthesis route of PM substrate could be easily controlled in comparison to the high temperature preparation method of porous metal and ceramics. Based on the features of porous magnesia (PM) substrate component, Ag/AgCl semiconductor could be facily formed by the ion exchange between AgNO<sub>3</sub> and Phase 5 crystals (Mg<sub>3</sub>Cl(OH)<sub>5</sub>·4H<sub>2</sub>O). In Fig. 1b, it can be seen that Ag/AgCl particles were successfully formed. Furthermore, the high resolution ESEM and BSEM images of Ag/AgCl/TiO<sub>2</sub>/PM sample (Fig. 1c) indicated that TiO<sub>2</sub> particles, Ag/AgCl particles and needle like phase 5 crystals have an excellent connectivity and combination structure.

XPS photographs were employed to further demonstrate the surface elemental compositions and chemical status of Ag/AgCl/TiO<sub>2</sub>/PM photocatalytic material, as shown in Fig. 1d. The typical XPS survey pattern of TiO<sub>2</sub>/PM mainly illustrated the XPS spectra of Mg, Cl, O, Ti and C elements, however, compared to TiO<sub>2</sub>/PM sample, an extra Ag element peak was observed in Ag/AgCl/TiO<sub>2</sub>/PM sample. Moreover, the high resolution XPS spectra of Cl2p (198.7 eV, inset in Fig. 1d) obviously shift for Ag/AgCl/TiO<sub>2</sub>/PM sample compared to TiO<sub>2</sub>/PM sample (Cl2p = 199.1 eV), indicating the bound Cl<sup>-</sup> of phase 5 was partially deprived by Ag<sup>+</sup> for forming the more stable AgCl precipitation. The Ag3d peak can be deconvoluted into two sets of double peaks, of which Ag3d<sub>3/2</sub> peak (373 eV) was divided into two different peaks at 373.6 and 374.3 eV, whereas Ag 3d<sub>5/2</sub> peak (367 eV) was divided into 368.6 and 367.5 eV. According to the reports of Zhang<sup>22</sup> and Huang<sup>23</sup>, the peaks at 373.6 and 367.5 eV were attributed to metallic silver binding energy in Ag3d<sub>3/2</sub> and Ag 3d<sub>5/2</sub>, and the peaks at 374.3 and 368.6 eV were ascribed to the Ag3d<sub>3/2</sub> and Ag 3d<sub>5/2</sub> of Ag<sup>+</sup> in AgCl, indicating the Ag/AgCl had successfully been modified on TiO<sub>2</sub>/PM sample.

The BSEM image could well and exactly reflect the distribution and sizes of Ag/AgCl particles due to the enormous atomic coefficient difference between Ti and Ag. As shown in the inset of Fig. 2a, it is clear revealed that the bright Ag/AgCl particles became more and more on TiO<sub>2</sub>/PM surface with increasing Ag modification contents from 0.70 × 10<sup>-4</sup> wt.% to 3.28 × 10<sup>-4</sup> wt.%. Meanwhile, the particle sizes also presented an irregular increase, when the Ag modification content achieved in 3.28 × 10<sup>-4</sup> wt.%, the biggest Ag/AgCl particle exceeded 500 nm, this may be due to the self-aggregation effect of metallic silver. Fig. 2a also shows the UV-vis diffuse reflectance spectra of TiO<sub>2</sub>/PM sample and various Ag/AgCl/TiO<sub>2</sub>/PM samples. It can be seen that TiO<sub>2</sub>/PM sample shows a strong absorption in UV light region. Furthermore, compared to the TiO<sub>2</sub>/PM sample, Ag/AgCl modified samples not only show stronger light absorption in the range of 200–400 nm, but also have substantial absorption in visible region (380–800 nm). These may be caused by the direct and indirect band gap of AgCl (3.25 eV), and the SPR of Ag nanoparticles<sup>24</sup>. In fact, the unique SPR peaks of Ag nanoparticles on AgCl surface are greatly influenced by their shapes and diameters, therefore various Ag nanoparticles lead to broad SPR peaks, which covered a wide visible light absorption range, and this is in good agreement with inset BSEM images.

The prepared samples are expected to have excellent photocatalytic activity for the degradation of organic contaminants due to their intense gas and light absorption performance. Fig. 2b shows the photocatalytic degradation of gaseous benzene using various samples. It can be observed that the photocatalytic performance of modified material increased gradually with increasing Ag modification contents. More specifically, Ag/AgCl/TiO<sub>2</sub>/PM with 3.28 × 10<sup>-4</sup> wt.% Ag content processed the highest photocatalytic activity for the decomposing of gaseous benzene, its reaction rate ( $k = 2.36 \times 10^{-2} \text{ min}^{-1}$ ) was 5.21 times and 30.57 higher than that of TiO<sub>2</sub>/PM and TiO<sub>2</sub>/imporous magnesian substrate sample (Table 1), indicating that the PM substrate micro structure and catalyst modification play important roles in enhancing the photocatalytic activity of TiO<sub>2</sub> particles. On one hand, the features of PM substrate like abundant pores, perforated cell walls and interlaced network structure were investigated to be useful for increasing TiO<sub>2</sub> coating areas, gas diffusion and light transmittance channels, therefore providing more reaction sites between TiO<sub>2</sub> particles and gaseous molecules, and ultimately enhancing photocatalytic efficiency<sup>20,25</sup>. On other hand, TiO<sub>2</sub> photocatalyst can be excited the photogenerated electron-hole pairs (e<sub>0</sub><sup>-</sup>-h<sup>+</sup>) under UV light, Ag nanoparticles on the surface of TiO<sub>2</sub> also could absorb the UV light and partial visible light for generating the (e<sub>1</sub><sup>-</sup>-Ag<sup>+</sup>) pairs. In that case, although partial e<sub>0</sub><sup>-</sup> could react with Ag<sup>+</sup> to form Ag, a majority of e<sub>0</sub><sup>-</sup> and e<sub>1</sub><sup>-</sup> would transfer to the surface of photocatalyst due to the enhanced local electric-field intensity by the Ag/AgCl<sup>26,27</sup>. Therefore, the more photogenerated electrons could facilitate the trapping of O<sub>2</sub> molecules for forming more superoxide ions (•O<sub>2</sub><sup>-</sup>) and other oxygen species, which contributes to the improvement of photocatalytic performance. Meanwhile, the photogenerated holes (h<sup>+</sup>) could react with AgCl and OH<sup>-</sup> to form Ag<sup>+</sup>, Cl<sup>0</sup> and •OH, respectively, in which Cl<sup>0</sup> and •OH could effective degrade organic pollutants, thus the photocatalytic performance could be further enhanced.

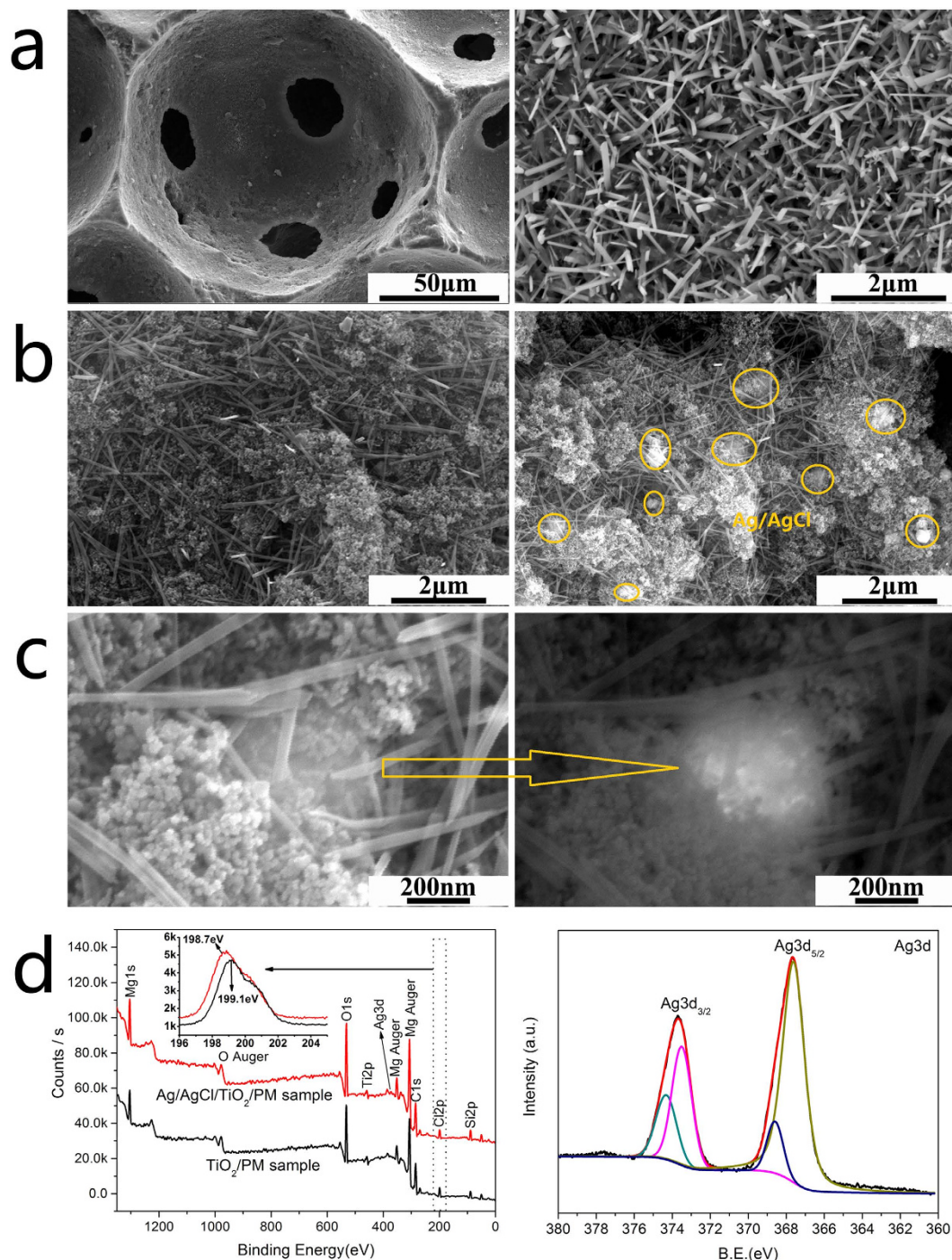


**Figure 1. Characterization of porous magnesium (PM), TiO<sub>2</sub>/PM and Ag/AgCl/TiO<sub>2</sub>/PM samples.** (a) Typical ESEM images of porous magnesium (PM) substrate. (b) Typical ESEM images of TiO<sub>2</sub>/PM and Ag/AgCl/TiO<sub>2</sub>/PM sample. (c) Typical high resolution ESEM and BSEM images of Ag/AgCl/TiO<sub>2</sub>/PM sample (2.34 × 10<sup>-4</sup> wt.% Ag content). (d) Typical XPS photographs of TiO<sub>2</sub>/PM and Ag/AgCl/TiO<sub>2</sub>/PM (2.34 × 10<sup>-4</sup> wt.% Ag content), the left image is survey pattern and Cl2p spectra (inset), the right image is high resolution XPS spectra image of Ag3d.

## Discussion

It is very interesting and meaningful to investigate the potential integration synthesis and catalytic mechanism of Ag/AgCl/TiO<sub>2</sub>/PM photocatalytic materials. It is well known that the main conditions and steps of photocatalytic reaction include: (1) interface contact and absorption between photocatalyst and pollutants; (2) appropriate light energy irradiating on photocatalyst surface; (3) pollutants be decomposed on photocatalyst surface; (4) desorption of decomposition products on photocatalyst surface. Among them, it is clear that the absorption ability and photocatalytic activity of photocatalytic materials play important roles in improving the removal effects of

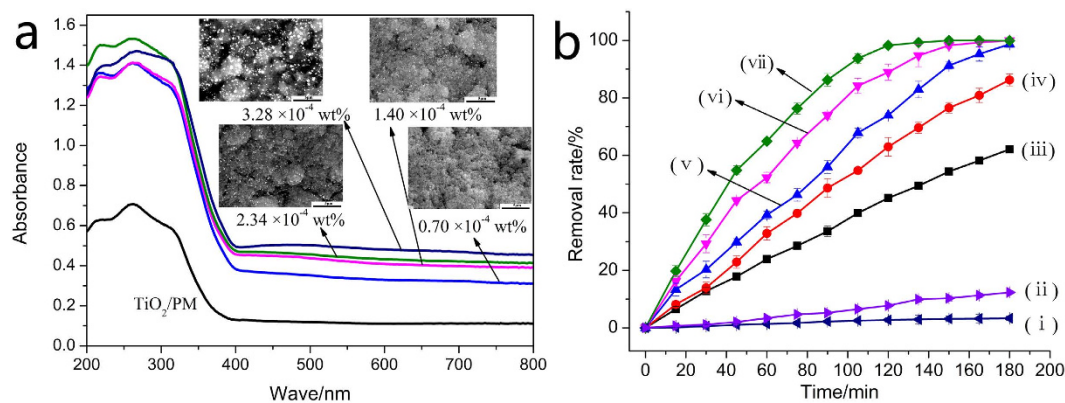


**Figure 2. Comparative light absorption ability and photocatalytic performance of various samples.** (a) UV-vis diffuse reflectance spectra of TiO<sub>2</sub>/PM and Ag/AgCl/TiO<sub>2</sub>/PM with various Ag modification contents ((0.7, 1.4, 2.34, 3.28) × 10<sup>-4</sup> wt.%), the inset images are corresponding BSEM images of Ag/AgCl/TiO<sub>2</sub>/PM samples. (b) Photocatalytic removal of benzene by various samples: (i) No catalytic; (ii) TiO<sub>2</sub>/imporous magnesian sample; (iii) TiO<sub>2</sub>/PM sample; (iv) ~ (v): Ag/AgCl/TiO<sub>2</sub>/PM sample with (0.7, 1.4, 2.34, 3.28) × 10<sup>-4</sup> wt.% Ag content.

Sample	Reaction rate ( $k/\text{min}^{-1}$ , 90 min)	Half-time ( $t_{1/2}/\text{min}$ )	Relativity ( $R^2$ )
(i)	$2.55 \times 10^{-4}$	–	0.9987
(ii)	$7.72 \times 10^{-4}$	897.7	0.9893
(iii)	$4.53 \times 10^{-3}$	153.0	0.9994
(iv)	$7.63 \times 10^{-3}$	90.8	0.9809
(v)	$9.78 \times 10^{-3}$	70.9	0.9886
(vi)	$1.81 \times 10^{-2}$	38.3	0.9835
(vii)	$2.36 \times 10^{-2}$	29.4	0.9727

**Table 1. The reaction rate of gaseous benzene removal by various samples.**

pollutants. In this study, the phase 5 as a main hydration product of PM substrate, is composed with triple chains octahedral (one Mg(OH)<sub>6</sub> and two Mg(OH)<sub>3</sub>(OH)<sub>2</sub>, or Mg(OH)<sub>4</sub>(OH)<sub>2</sub> octahedra along axis b infinite extension) and the chains of intercalating Cl atoms and water molecules (SOF = 0.500, Fig. 3a), which means that phase 5 structure could be controlled by Mg-O octahedral amounts<sup>28</sup>. Thus, as shown in Figs 1a and 3a,b, through introducing bubbles and controlling the mixture ratios of MgO and MgCl<sub>2</sub> solution, the amounts of Phase 5 and its accumulation structure could be regulated easily. Furthermore, by using the negative pressure coating method, TiO<sub>2</sub> particles could be filled into phase 5 interlaced network pores (Figs 1b and 3b), which would obviously improve the contact areas between TiO<sub>2</sub> particles with light energy and pollutants. As shown in Fig. 3c, the isotherm of TiO<sub>2</sub>/PM sample provided more specific results about those inference. It can be seen that the isotherm of TiO<sub>2</sub>/PM sample had one hysteresis loop at relative pressure between 0.43 and 1, demonstrated that it was mesoporous structures. Particularly, in 0.9~1.0 high pressure regions, the absorption volume rising faster indicated that the material contained macro pores. The inset pore size distribution curves also revealed that TiO<sub>2</sub>/PM had an obvious pore peaks in the range of 1~100 nm. Those could offer the gas diffusion and light transmittance channels from the particle surface to the interior, which are expected to be useful in the photocatalytic process.

More importantly, as shown in Fig. 3a,b, the Cl ion resource of PM substrate could simultaneously provide the effective and facile modification method for the formation of Ag/AgCl semiconductor, which was proved by the results of Fig. 1b–d, means the light absorption performance and charges transfer properties of TiO<sub>2</sub> particles could be enhanced by Ag/AgCl/TiO<sub>2</sub> composite structure. Furthermore, as shown in Fig. 2a, it also can be seen that the UV-Vis spectral data for the Ag/AgCl/TiO<sub>2</sub>/PM sample (3.28 × 10<sup>-4</sup> wt.% Ag content) shows higher absorption from UV to Vis light regions compared to other controls. Overall, based on PM substrate special physical structure coupling with its chemical *in situ* Ag/AgCl modification method to TiO<sub>2</sub> particles, the high-activity Ag/AgCl/TiO<sub>2</sub>/PM photocatalytic composite material was explored, which shown the higher photocatalytic efficiency for the decomposing of gaseous benzene compared to other controls (Fig. 2b and Table 1). This may provide a new strategy for high-efficiency application of TiO<sub>2</sub> photocatalyst in building materials field.

In conclusions, based on hierarchical porous magnesian substrate coupling with its chemical *in situ* Ag/AgCl modification method to TiO<sub>2</sub> particles, the high-activity Ag/AgCl/TiO<sub>2</sub>/PM photocatalytic composite material was explored. The sample revealed excellent photocatalytic removal performance on gaseous benzene. More

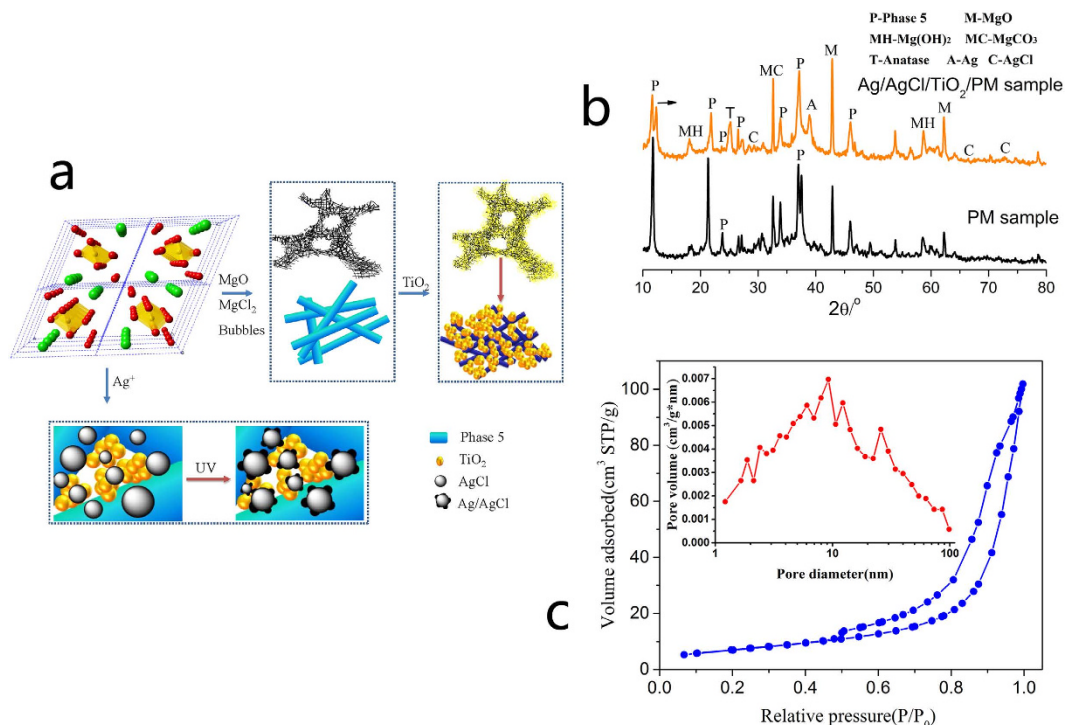


**Figure 3. The *in situ* synthesis and photocatalytic performance mechanism analysis of Ag/AgCl/TiO<sub>2</sub>/PM sample.** (a) The integration synthesis schematic of Ag/AgCl/TiO<sub>2</sub>/PM sample. (b) XRD patterns of PM sample and Ag/AgCl/TiO<sub>2</sub>/PM sample with  $2.34 \times 10^{-4}$  wt.% Ag content. (c) Typical N<sub>2</sub> adsorption-desorption isotherms and pore size distribution of TiO<sub>2</sub>/PM sample.

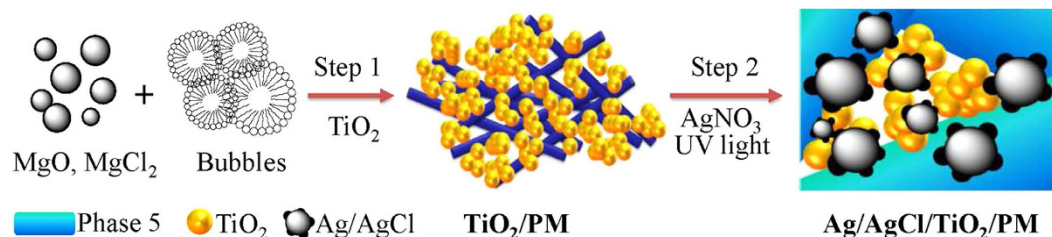


**Figure 4. Schematic diagram illustrating the preparation of sample.** Step 1: preparation of PM substrate; Step 2: synthesis of Ag/AgCl/TiO<sub>2</sub>/PM sample.

specifically, Ag/AgCl/TiO<sub>2</sub>/PM with  $3.28 \times 10^{-4}$  wt.% Ag content processed the highest photocatalytic activity for the decomposing of gaseous benzene, its reaction rate ( $k = 2.36 \times 10^{-2} \text{ min}^{-1}$ ) was 5.21 and 30.57 times higher than that of TiO<sub>2</sub>/PM and TiO<sub>2</sub>/imporous magnesian substrate, respectively. The integration synthesis and photocatalysis mechanism of Ag/AgCl/TiO<sub>2</sub>/PM composite material were investigated. The PM substrate which is composed with phase 5 crystals (Mg<sub>3</sub>Cl(OH)<sub>5</sub>·4H<sub>2</sub>O) offered well gas diffusion and light transmittance channels for photocatalysis. Moreover, with the Cl<sup>-</sup> resource of phase 5 crystals, the Ag/AgCl/TiO<sub>2</sub>/PM composite structure was simultaneously synthesized by *in situ* method, which enhanced the light absorption response and charge transfer properties of TiO<sub>2</sub> particles. Therefore, the synthesis method and prepared material in this paper provide a novel strategy for high-efficiency application of TiO<sub>2</sub> photocatalyst in engineering filed.

## Methods

**Chemicals and reagents.** Magnesium oxide (MgO, analytically pure, Liaoning Ying kou Co., Ltd), magnesium chloride (MgCl<sub>2</sub>·6H<sub>2</sub>O, analytically pure, Liaoning Ying kou Co., Ltd), bone glue protein foaming agent with solid content of 36%, specific gravity of 1.16g/cm<sup>3</sup>, PH of 9~10, was purchased from Henan Province (Yongtai co. ltd, technical grade), China. Degussa P25 (20% rutile and 80% anatase) with 99.5% purity and 30 nm particle size was used as TiO<sub>2</sub> photocatalyst. Silver nitrate (AgNO<sub>3</sub>) and absolute alcohol (C<sub>2</sub>H<sub>5</sub>OH) were analytical reagents, which were provided by Shenshi Chem.

**Photocatalytic materials synthesis.** Porous magnesian (PM) substrate was prepared through a sample method. As shown in Fig. 4 (Step 1), in a typical preparation, 43 g magnesium oxide powder and 57 g MgCl<sub>2</sub> water

solution (w% = 27.4%) were added into 500 mL polytetrafluoroethylene beaker stirring 3 min. Then 200 mL bubbles with  $(0.04 \pm 0.005) \text{ g/cm}^3$  volume density was added, and stirring 2 min to form PM fresh slurry. The bubbles was prepared with 3 mL foaming agent and 50 mL deionized water by mechanical stirring method (2000 r/min). After that, casted PM fresh slurry into silicone moulds, and aging 28 d in the temperature at  $(20 \pm 1)^\circ\text{C}$  and relative humidity at  $(60 \pm 5)\%$ , then the PM sample was demoulded and cut into slices of  $\Phi 160 \times 3 \text{ mm}$ . Subsequently, the slice was cleaned by compressed air and placed in the oven at  $65^\circ\text{C}$ . The synthesis of Ag/AgCl/TiO<sub>2</sub>/PM sample was achieved by self-assembly and photo-reduction method (Fig. 4 (Step 2)). Firstly, PM substrate was put into vacuum saturation apparatus and loading 0.1 MPa vacuum 30 min at room temperature, 500 mL 1 g/L TiO<sub>2</sub> absolute alcohol dispersion solution was inhaled into the above container with a stirring to keep the homogeneous suspension solution, after 1 h, TiO<sub>2</sub>/PM precursor was taken out, and washed by distilled water, and then dried in oven at  $85^\circ\text{C}$ . Secondly, a certain amount of AgNO<sub>3</sub> ethanol-water solution (ethanol/water volume ratio = 3/1,  $C_{\text{AgNO}_3} = 5.0 \times 10^{-3} \text{ mol/L}$ ) was sprayed on TiO<sub>2</sub>/PM surface for 30 min, and then the prepared sample was irradiated under 300 W high pressure Hg lamp (China, Shanghai Yaming, GYZ,  $\lambda_{\text{nm}} > 340 \text{ nm}$ , the light spectrum with peaks around 365, 400, 440, 550 and 580 nm) for 10 min. After that, the resulting sample was washed with 65% ethanol-water solution (volume ratio), and finally dried at  $85^\circ\text{C}$  for 4 h. Ag/AgCl/TiO<sub>2</sub>/PM samples were denoted by mass fraction of Ag to TiO<sub>2</sub>/PM (Ag wt.%), the weight of Ag was calculated by AgNO<sub>3</sub> spraying amount.

**Characterization and Photocatalytic performance.** The crystalline phases of samples were determined by X-ray diffractometer (XRD, PHILIPS P W 3040/60X PertPRO) with a Cu K $\alpha$  ray source. Environmental Scanning electron microscopy (ESEM, Quanta FEG 450, FEI) together with a Backscattered electron (BSE) detector were used to observe the morphology of samples. X-ray Photoelectron Spectrometer (V. G. Scientific Ltd; Al K Alpha) test was carried out to obtain the chemical state of element and bonding energy. UV-vis diffuse reflectance spectra were recorded in diffuse reflectance mode (R) and transformed to absorption spectra through the Kubelka-Munk function<sup>29,30</sup>. A Lambda 35 (PerkinElmer) spectrometer equipped with a Labsphere RSA-PE-20 integration sphere and MgO as a standard were used. N<sub>2</sub> adsorption-desorption isotherms were measured on an ASAP 2020 instrument (Micromeritics, USA). The photocatalytic performance was evaluated by removal of gaseous benzene in a closed cylindrical stainless steel gas-phase reactor (2.35 L) with a quartz window. The light source is a 300 W high pressure Hg lamp (China, Shanghai Yaming, GYZ,  $\lambda_{\text{max}} \approx 365 \text{ nm}$ ), the distance between the lamp and the sample surface was 35 cm. 2  $\mu\text{l}$  of benzene liquid was injected in the reactor, and the mixture was irradiated by the light as the liquid benzene completely evaporated into gaseous. The samples were measured every 5 min by gas chromatograph (GC2020, Wuhan, Hengxin, which equipped with a flame ionization detector, a methane converter). For repeated photocatalytic performance test, after each photocatalysis, the photocatalyst was irradiated under UV-C lamp (Philips, 36W,  $\lambda_{\text{max}} = 254 \text{ nm}$ ) for 24 h to completely decompose the absorbed gaseous benzene molecules. Then, covered the reactor again, 2  $\mu\text{l}$  of benzene was injected in the reactor, and the Hg lamp was turned on to start the next test. Each procedure was repeated three times and the data were given as the arithmetic mean standard deviation. The degradation rate and reaction rate were calculated by as following formulas:

$$\eta\% = \frac{C_0 - C_t}{C_0} \times 100\% \quad (1)$$

$$\ln\left(\frac{C_t}{C_0}\right) = -kt \quad (2)$$

where  $C_t$  and  $C_0$  are the concentrations of the primal and remaining benzene,  $k$  is the reaction rate;  $t$  is the light illumination time.

## References

- Hoffmann, M. R., Martin, S. T., Choi, W. & Bahnemann, D. W. Environmental Applications of Semiconductor Photocatalysis. *Chemical Reviews* **95**, 69–96 (1995).
- Banerjee, A. The design, fabrication, and photocatalytic utility of nanostructured semiconductors: focus on TiO<sub>2</sub>-based nanostructures. *Nanotechnology, Science and Applications*. **35** (2011).
- Aissa, A. H. *et al.* Characterization and photocatalytic performance in air of cementitious materials containing TiO<sub>2</sub>. Case study of formaldehyde removal. *Applied Catalysis B-Environmental* **107**, 1–8 (2011).
- Serpone, N. & Emeline, A. V. Semiconductor photocatalysis: past, present, and future outlook. *The Journal of Physical Chemistry Letters* **3**, 673–677 (2012).
- Hanus, M. J. & Harris, A. T. Nanotechnology innovations for the construction industry. *Progress in Materials Science* **58**, 1056–1102 (2013).
- Tong, H. *et al.* Nano-photocatalytic materials: possibilities and challenges. *Advanced materials* **24**, 229–251 (2012).
- Ye, L. *et al.* Two Different Roles of Metallic Ag on Ag/AgX/BiOX (X = Cl, Br) Visible Light Photocatalysts: Surface Plasmon Resonance and Z-Scheme Bridge. *ACS Catalysis* **2**, 1677–1683 (2012).
- Tang, Y. *et al.* Efficient Ag@AgCl Cubic Cage Photocatalysts Profit from Ultrafast Plasmon Induced. *Advanced Functional Materials* **23**, 2932–2940 (2013).
- Tian, B. *et al.* Sandwich-structured AgCl@Ag@TiO<sub>2</sub> with excellent visible-light photocatalytic activity for organic pollutant degradation and E. coli K12 inactivation. *Applied Catalysis B: Environmental* **158–159**, 76–84 (2014).
- Wang, D. *et al.* Ag/AgCl@helical chiral TiO<sub>2</sub> nanofibers as a visible-light driven plasmon photocatalyst. *Chemical communications* **49**, 10367–10369 (2013).
- Ingram, D. B. & Linic, S. Water splitting on composite plasmonic-meta/semiconductor photoelectrodes: Evidence for selective plasmon-induced formation of charge carriers near the semiconductor surface. *Journal of American Chemistry Society* **133**, 5202–5205 (2011).

12. Belloni, J., Treguer, M., Remita, H. & De Keyser, R. Enhanced yield of photoinduced electrons in doped silver halide crystals. *Nature* **402**, 865–867 (1999).
13. Wang, X. E. A. A metal-free polymeric photocatalyst for hydrogen production from water under visible light. *Natural materials* **8**, 76–80 (2009).
14. Shah, Z. H. *et al.* Highly enhanced plasmonic photocatalytic activity of Ag/AgCl/TiO<sub>2</sub> by CuO co-catalyst. *Journal of Materials Chemistry A* **3**, 3568–3575 (2015).
15. Jimenez-Relinque, E., Rodriguez-Garcia, J. R., Castillo, A. & Castellote, M. Characteristics and efficiency of photocatalytic cementitious materials: Type of binder, roughness and microstructure. *Cement and Concrete Research* **71**, 124–131 (2015).
16. Kamperman, M. *et al.* Integrating Structure Control over Multiple Length Scales in Porous High Temperature Ceramics with Functional Platinum Nanoparticles. *Nano Letters* **9**, 2756–2762 (2009).
17. Parlett, C. M. A., Wilson, K. & Lee, A. F. Hierarchical porous materials: catalytic applications. *Chemical Society Reviews* **43**, 3876–3893 (2013).
18. Visa, M., Isac, L. & Duta, A. Fly ash adsorbents for multi-cation wastewater treatment. *Applied Surface Science* **258**, 6345–6352 (2012).
19. Chen, J. & Poon, C.-S. Photocatalytic construction and building materials: From fundamentals to applications. *Building and Environment* **44**, 1899–1906 (2009).
20. Wang, F., Yang, L., Sun, G., Guan, L. & Hu, S. The hierarchical porous structure of substrate enhanced photocatalytic activity of TiO<sub>2</sub>/cementitious materials. *Construction and Building Materials* **64**, 488–495 (2014).
21. Wang, F., Yang, L., Guan, L. & Hu, S. Microstructure and properties of cement foams prepared by magnesium oxychloride cement. *J. Wuhan Univ. Technol.-Mat. Sci. Edit.* **30**, 331–337 (2015).
22. McEvoy, J. G., Cui, W. Q. & Zhang, Z. S. Synthesis and characterization of Ag/AgCl-activated carbon composites for enhanced visible light photocatalysis. *Applied Catalysis B-Environmental* **144**, 702–712 (2014).
23. Chen, H., Xiao, L. & Huang, J. Template synthesis of Ag/AgCl microrods and their efficient visible light-driven photocatalytic performance. *Materials Research Bulletin* **57**, 35–40 (2014).
24. Linic, S., Christopher, P. & Ingram, D. B. Plasmonic-metal nanostructures for efficient conversion of solar to chemical energy. *Nature Materials* **10**, 911–921 (2011).
25. Wang, F., Yang, L., Wang, H. & Yu, H. Facile preparation of photocatalytic exposed aggregate concrete with highly efficient and stable catalytic performance. *Chemical Engineering Journal* **264**, 577–586 (2015).
26. Wang, P. *et al.* Highly Efficient Visible-Light Plasmonic Photocatalyst Ag@AgBr. *Chemistry – A European Journal* **15**, 1821–1824 (2009).
27. Guo, J. F., Ma, B., Yin, A., Fan, K. & Dai, W. L. Highly stable and efficient Ag/AgCl@TiO<sub>2</sub> photocatalyst: preparation, characterization, and application in the treatment of aqueous hazardous pollutants. *Journal of hazardous materials* **211–212**, 77–82 (2012).
28. Sugimoto, K., Dinnebier, R. E. & Schlecht, T. Structure determination of Mg<sub>3</sub>(OH)<sub>5</sub>Cl·4H<sub>2</sub>O (F5 phase) from laboratory powder diffraction data and its impact on the analysis of problematic magnesia floors. *Acta Crystallographica Section B* **63**, 805–811 (2007).
29. Kato, H. & Kudo, A. Visible-light-response and photocatalytic activities of TiO<sub>2</sub> and SrTiO<sub>3</sub> photocatalysts codoped with antimony and chromium. *Journal of Physical Chemistry B* **106**, 5029–5034 (2002).
30. Yang, L., Liu, P., Li, X. & Li, S. The photo-catalytic activities of neodymium and fluorine doped TiO<sub>2</sub> nanoparticles. *Ceramics International* **38**, 4791–4796 (2012).

## Acknowledgements

We gratefully acknowledge the financial support by the EPSRC-NSFC Joint Research Project (No. 51461135005) and National Natural Science Foundation (No. 51478370) of China.

## Author Contributions

L.Y. and F.W. developed the project, carried out the experimental work, and analyzed results. C.S. assisted with the photocatalytic performance measurement. P.L., W.Z. and S.H. assisted with analysis.

## Additional Information

**Competing financial interests:** The authors declare no competing financial interests.

**How to cite this article:** Yang, L. *et al.* An *in-situ* synthesis of Ag/AgCl/TiO<sub>2</sub>/hierarchical porous magnesian material and its photocatalytic performance. *Sci. Rep.* **6**, 21617; doi: 10.1038/srep21617 (2016).



This work is licensed under a Creative Commons Attribution 4.0 International License. The images or other third party material in this article are included in the article's Creative Commons license, unless indicated otherwise in the credit line; if the material is not included under the Creative Commons license, users will need to obtain permission from the license holder to reproduce the material. To view a copy of this license, visit <http://creativecommons.org/licenses/by/4.0/>